Interplays between State and Flux Hydrological Variables across Vadose Zones: A Numerical Investigation

Zhaoxin Wang [1], Tiejun Wang [1,2,*] and Yonggen Zhang [1,2]

[1]   Institute of Surface-Earth System Science, Tianjin University, Weijin Road 92, Tianjin 300072, China; wangzhaoxin@tju.edu.cn (Z.W.); ygzhang@tju.edu.cn (Y.Z.)

[2]   Tianjin Key Laboratory of Earth Critical Zone Science and Sustainable Development in Bohai Rim, Tianjin University, Weijin Road 92, Tianjin 300072, China

*   Correspondence: tiejun.wang@tju.edu.cn

Abstract: Knowledge of both state (e.g., soil moisture) and flux (e.g., actual evapotranspiration (ET_a) and groundwater recharge (GR)) hydrological variables across vadose zones is critical for understanding ecohydrological and land-surface processes. In this study, a one-dimensional process-based vadose zone model with generated soil hydraulic parameters was utilized to simulate soil moisture, ET_a, and GR. Daily hydrometeorological data were obtained from different climate zones to drive the vadose zone model. On the basis of the field phenomenon of soil moisture temporal stability, reasonable soil moisture spatiotemporal structures were reproduced from the model. The modeling results further showed that the dependence of ET_a and GR on soil hydraulic properties varied considerably with climatic conditions. In particular, the controls of soil hydraulic properties on ET_a and GR greatly weakened at the site with an arid climate. In contrast, the distribution of mean relative difference (MRD) of soil moisture was still significantly correlated with soil hydraulic properties (most notably residual soil moisture content) under arid climatic conditions. As such, the correlations of MRD with ET_a and GR differed across different climate regimes. In addition, the simulation results revealed that samples with average moisture conditions did not necessarily produce average values of ET_a and GR (and vice versa), especially under wet climatic conditions. The loose connection between average state and flux hydrological variables across vadose zones is partly because of the high non-linearity of subsurface processes, which leads to the complex interactions of soil moisture, ET_a, and GR with soil hydraulic properties. This study underscores the importance of using soil moisture information from multiple sites for inferring areal average values of ET_a and GR, even with the knowledge of representative sites that can be used to monitor areal average moisture conditions.

Keywords: soil moisture; groundwater recharge; evapotranspiration; vadose zone; soil hydraulic property; climate

1. Introduction

Estimation of state (e.g., soil moisture) and flux (e.g., actual evapotranspiration (ET_a) and groundwater recharge (GR)) hydrological variables across vadose zones are of great importance for many research and application purposes, and especially for understanding ecohydrological and land-surface processes in Earth's critical zones [1–3]. Due to the high non-linearity and extreme complexity of hydrological systems, those state and flux variables tend to display significant spatiotemporal variability. For example, a wealth of field and numerical studies has shown that there was considerable variability in soil moisture at different spatiotemporal scales, as a result of its complex interactions with surrounding environments [4,5]. Likewise, flux hydrological variables, such as ET_a and GR,

may also vary substantially across landscapes, largely because of the marked spatial variations in soil texture, vegetation, and climatic conditions [1,6–9]. As such, accurate estimation of those state and flux variables presents grand challenges to scientific communities [10–13]. Given the tight connections between state and flux variables [12,14,15], it is thus imperative to elucidate the interplays among those variables to improve their estimation across vadose zones.

To enhance the representativeness of estimation of state and flux hydrological variables across vadose zones, various techniques have been developed [6,16,17]. Notably, in the field of soil hydrology, the method of temporal stability analysis (*TSA*) initially proposed by Vachaud et al. [18] has been widely adopted to identify representative locations for monitoring soil moisture conditions [19]. Based on field observations, Vachaud et al. [18] found that there was a temporal persistence in the spatial structure of soil moisture. Specifically, Vachaud et al. [18] showed that soil moisture levels at certain locations in a field were closer to the areal average moisture conditions, whereas other locations consistently displayed either drier or wetter conditions than the areal average moisture conditions. As such, Vachaud et al. [18] suggested that it was feasible to apply the *TSA* method, which is based on the metric of mean relative difference (*MRD*) of soil moisture (an indicator of the relative wetness at a location as compared to the areal average wetness), to seek representative sites for monitoring areal average moisture conditions (e.g., sites with *MRD* values closest to zero). Since the seminal work of Vachaud et al. [18], the use of the *TSA* method has also been extended to optimize soil moisture monitoring networks, diagnose soil moisture spatiotemporal patterns, fill missing soil moisture data, and improve the practice of water resources management [20–24].

Despite its wide applications, the implication of the *TSA* method for understanding flux hydrological variables across vadose zones has not been adequately addressed. In general, the availability of field measurements of ET_a and *GR* is extremely limited due to the high operational and maintenance costs of measurement equipment [3,25]. As an effective alternative to resolve this issue, soil moisture data have been used to infer ET_a and *GR*, such as through inverse modeling [15,26,27]. Given the significant spatial variability in ET_a and *GR*, it naturally leads to the question as to whether soil moisture data from representative locations identified by the *TSA* method can be used to infer areal average values of ET_a and *GR*. To answer this question, it requires the knowledge of the relationships of soil moisture with ET_a and *GR*. Although previous modeling studies have revealed that soil moisture, ET_a, and *GR* were affected by similar factors (e.g., soil, vegetation, and climate), the dependence of those variables on environmental factors might vary considerably [9,28,29]. Therefore, further investigation into the interplays among soil moisture, ET_a, and *GR* is still warranted.

The primary goals of this study were two-fold: (1) to investigate the relationships of soil moisture with ET_a and *GR* under different climatic conditions and (2) to examine whether soil samples with average moisture conditions can also produce average hydrological fluxes, such as ET_a and *GR*, across vadose zones. To this end, a commonly used process-based vadose zone model with generated soil hydraulic parameters was utilized to simulate soil moisture, ET_a, and *GR*, as this type of modeling approach has been widely adopted for understanding hydrological processes across vadose zones (e.g., Vereecken et al. [30]; Wang et al. [31]; Martinez et al. [28]; also see the review by Vereecken et al. [5]). Based on the simulation results, the distribution patterns of *MRD*, ET_a, and *GR* were first discussed, and then the correlations of *MRD* with ET_a and *GR* were examined to understand the interdependence of those variables on climatic conditions and soil hydraulic properties. Finally, with the aid of the *TSA* method, the feasibility of using representative locations of soil moisture for estimating areal average values of ET_a and *GR* was evaluated.

2. Methods and Materials

2.1. Model Setup and Data Inputs

The widely used Hydrus-1D model [32] was employed in this study to simulate soil moisture, ET_a, and *GR*, due to the accuracy of its numerical algorithm [33]. The Hydrus-1D model is a one-dimensional

process-based vadose zone model, which utilizes the Richards equation to simulate soil water movement in vadose zones:

$$\frac{\partial \theta}{\partial t} = \frac{\partial}{\partial x}\left[K(h)\left(\frac{\partial h}{\partial x}\right) - K(h)\right] - S(h) \tag{1}$$

where θ (L^3/L^3) is volumetric soil moisture content, t (T) is time, x (L) is spatial coordinate, h (L) is pressure head, K (L/T) is hydraulic conductivity, and S (1/T) is a sink/source term (e.g., root water uptake). To be concise, only brief information on the model setup is given here, and detailed mathematical descriptions of the simulated processes can be found in Simunek et al. [32]. Specifically, the length of the simulated soil columns was set to be 3 m with a total of 301 spatial nodes evenly distributed at 1 cm intervals. Additional numerical experiments showed that further increases in the number of the spatial nodes did not improve the simulation results. At the surface, an atmospheric boundary condition was chosen for calculating actual soil evaporation (E_a), which primarily depended on potential soil evaporation (E_p) and a predefined pressure head at the surface [34]. Surface runoff was allowed to occur when precipitation (P) intensity was greater than the soil infiltration capacity or the surface soil layer became saturated. A unit hydraulic gradient condition was imposed at the lower boundary of the simulated soil columns. As such, GR is defined here as the amount of water that passes downward across the lower boundary [6,31].

The method of Feddes et al. [35] was used to compute root water uptake, which depended on potential transpiration (T_p), soil matric potential, and root density distribution. Note that root water uptake was assumed to be equal to actual transpiration (T_a) in this study. Daily potential transpiration T_p was obtained by partitioning daily potential evapotranspiration (ET_p) into T_p and E_p according to Beer's law [36]:

$$E_p = ET_p \times e^{-k \times LAI} \tag{2}$$

$$T_p = ET_p - E_p \tag{3}$$

where k is an extinction coefficient (0.5 in this study) and LAI is leaf area index. Following Wang and Zlotnik [37], LAI data were retrieved from the MODIS_MOD15 dataset [38] based on the geographical coordinates of the study sites. The exponential model of Jackson et al. [39] was adopted to describe the root density distribution according to the vegetation types at the study sites. Finally, the sum of E_a and T_a was set to be equal to ET_a.

Instead of generating synthetic data to drive the Hydrus-1D model [28,40], five years of daily hydrometeorological data from four study sites with contrasting hydroclimatic conditions across China were obtained from the National Centers for Environmental Information [41], including Hangzhou, Guiyang, Tianjin, and Yinchuan. Specifically, the climates at Hangzhou and Guiyang are humid and sub-humid, respectively. By comparison, Tianjin is located in a semi-arid climate zone, while Yinchuan is located in an arid climate zone. First, daily P and maximum and minimum air temperatures were retrieved for each site. Given the data availability, the Hargreaves equation was used to calculate daily ET_p based on maximum and minimum air temperatures [42]. The summary of mean annual P ($\overline{P}$) and mean annual ET_p ($\overline{ET_p}$) during the study period is provided in Table 1 for the four sites. Based on the land cover of the study sites, forest was assumed at Hangzhou and Guiyang, while grass and shrub were assumed at Tianjin and Yinchuan, respectively. Physiological parameter values for different vegetation types, which were used for computing root water uptake, were obtained from literature [43–45]. Finally, to minimize the impact of initial conditions on the simulation results, all simulations were repeated for four times (i.e., a total of 20 years) until the simulated soil moisture profiles were in equilibrium with atmospheric forcings, and the simulation results from the last repetition were used in the analysis.

Table 1. Mean annual precipitation ($\overline{P}$), potential evapotranspiration ($\overline{ET_p}$), and aridity index ($\overline{ET_p/P}$) at the study sites.

Location	Latitude	Longitude	$\overline{P}$ (cm/year)	$\overline{ET_p}$ (cm/year)	$\overline{ET_p/P}$(-)
Hangzhou	30.23°N	120.17°E	150.9 (127.4–172.9) *	111.8 (108.0–115.1)	0.74 (0.62–0.89)
Guiyang	26.58°N	106.73°E	103.8 (73.5–137.1)	101.7 (95.9–104.6)	0.98 (0.74–1.40)
Tianjin	39.10°N	117.17°E	54.3 (35.6–75.7)	104.1 (99.9–107.2)	1.92 (1.37–2.81)
Yinchuan	38.47°N	106.20°E	20.8 (16.6–29.2)	108.6 (106.8–110.5)	5.22 (3.74–6.43)

* The range of annual values is given in the parentheses.

2.2. Generation of Soil Hydraulic Parameters

To solve Equation (1), the constitutive relations among θ, h, and K are required. In this study, the van Genuchten–Mualem (VGM) model [46,47] was utilized:

$$\theta(h) = \begin{cases} \theta_r + \dfrac{\theta_s - \theta_r}{(1+|\alpha h|^n)^m}, h < 0 \\ \theta_s, \quad h \geq 0 \end{cases} \tag{4}$$

$$K(h) = K_S \times S_e^{\,l} \times (1 - (1 - S_e^{1/m})^{\,m})^2 \tag{5}$$

where θ_r (L^3/L^3) and θ_s (L^3/L^3) are residual and saturated soil moisture content, respectively, K_S (L/T) is saturated hydraulic conductivity, and S_e (-) is effective saturation degree that is defined as $(\theta - \theta_r)/(\theta_s - \theta_r)$. The parameters α, n, and l are shape factors: α(1/L) is related to the inverse of air entry pressure, n (-) is a measure of pore size distributions with $m = 1 - 1/n$, and l (-) is a measure of pore tortuosity and connectivity.

In previous modeling studies, because of the lack of field data, synthetic soil hydraulic parameter datasets have been routinely used to characterize the spatial variability in soil hydraulic properties for simulating soil moisture, ET_a, and GR [9,28,48,49]. Here, the method of Zhang and Schaap [50] was utilized to generate the VGM parameters for loamy sand, sandy loam, and silt loam. This method is built on the assumption of either normal (θ_r and θ_s) or lognormal (α, n, and K_s) distributions of the VGM parameters. The validity of this assumption has been verified by Zhang and Schaap [50]. Based on a Monte Carlo procedure, new samples were drawn from the parameter (normal or lognormal) distributions with means and standard deviations given by Zhang and Schaap [50] for each soil texture class. In addition, following Wang et al. [31] and Zhang et al. [51], the parameter l was fixed to be 0.5 in all simulations. In this study, a total of 200 samples were generated for each soil texture class and the statistical summary of the generated VGM parameters is provided in Table 2. Note that soil profiles with uniform soil textures were used in this study. The main purpose of using uniform soil profiles is to promote general understanding, and thus reach general conclusions regarding the impact of soil hydraulic properties on subsurface hydrological processes. By comparison, the use of non-uniform soil profiles might lead to site-specific conclusions (as done in the majority of field-scale soil moisture studies), which, however, deserves future investigation based on numerical approaches.

Table 2. Average values of soil hydraulic parameters for the van Genuchten–Mualem model generated for different soil textural classes.

Soil Texture	θr (cm^3 cm^{-3})	θs (cm^3 cm^{-3})	α (1/cm)	n (-)	K_s (cm/day)
Loamy sand	0.064 (0.035) *	0.386 (0.063)	0.036 (0.039)	1.908 (0.580)	342.5 (864.1)
Sandy loam	0.076 (0.047)	0.381 (0.068)	0.040 (0.075)	1.673 (0.359)	125.4 (334.1)
Silt loam	0.098 (0.057)	0.432 (0.077)	0.006 (0.007)	1.790 (0.475)	62.8 (180.9)

* Standard deviation values are given in parenthesis.

2.3. Temporal Stability Analysis of Soil Moisture

Given its wide applications for analyzing soil moisture spatiotemporal patterns [19,52,53], the *TSA* method was adopted in this study to examine the relationships of soil moisture with ET_a and *GR*. The *TSA* method is based on the metric of relative difference (*RD*) of soil moisture, which is defined as:

$$RD_{ij} = \frac{\theta_{ij} - \overline{\theta}_j}{\overline{\theta}_j} \tag{6}$$

where θ_{ij} is soil moisture content at location *i* and time *j*, and $\overline{\theta}_j$ is the spatial average of soil moisture content at time *j*. With a series of *RD* over time, *MRD* at location *i* is given as:

$$MRD_i = \frac{1}{m} \sum_{j=1}^{m} RD_{ij} \tag{7}$$

where *m* is the number of observations over the study period. By definition, the term *MRD* characterizes the wetness condition at a location relative to the areal average wetness condition of the study field over the study period. Therefore, *MRD* can be used to characterize the spatial distribution of soil moisture (average state) and the sites with *MRD* values closest to zero can be selected as representative locations for monitoring field average moisture conditions [18,19].

The standard deviation of *RD* (*SDRD*) is another useful metric for quantifying soil moisture temporal dynamics and defined as:

$$SDRD_i = \left[\frac{1}{m-1} \sum_{j=1}^{m} \left(RD_{ij} - MRD_i \right)^2 \right]^{0.5} \tag{8}$$

According to its definition, sites with lower *SDRD* values indicate higher temporal stability of soil moisture than those with higher *SDRD* values. Note that instead of using soil moisture storage in this study, daily volumetric soil moisture content at 25 cm extracted from the last repetition of the simulations was analyzed. Since soil moisture storage is equivalent to depth-weighted soil moisture content and similar simulation results were obtained from other depths (e.g., 10, 50, and 100 cm), the conclusions made in this study essentially remain the same based on depth-specific simulation data. In addition, the use of depth-specific data is to be consistent with the framework set for soil moisture monitoring networks (e.g., Nebraska Mesonet, Oklahoma Mesonet, and Soil Climate Analysis Network), which report soil moisture data at different soil depths.

3. Results and Discussion

3.1. Comparison of Hydroclimatic Conditions across the Study Sites

The statistical summary of $\overline{P}$ and $\overline{ET_p}$ during the study period is reported in Table 1 for the study sites. Among the four sites, there was a significant gradient in $\overline{P}$ increasing from 20.8 cm/year at

Yinchuan to 150.9 cm/year at Hangzhou; whereas, the spatial variations in $\overline{ET_p}$ were much smaller with a range from 101.7 cm/year at Guiyang to 111.8 cm/year at Hangzhou. As a result, a wide range of mean annual aridity index (i.e., $\overline{ET_p}/\overline{P}$) existed across the sites, varying from 0.74 at Hangzhou to 5.22 at Yinchuan. Given the diversity of climate regimes among the selected sites (e.g., from arid to humid climates), mean annual ratios of ET_a (defined as $\overline{ET_a}/\overline{P}$) and GR ($\overline{GR}/\overline{P}$) were used in the following analysis to ensure the comparability of the simulated patterns of ET_a and GR at different sites. With regard to the interannual variability, there were also pronounced variations in annual P at all sites; however, the interannual variability in ET_p was less significant (Table 1). It should be noted that climate seasonality is another important climatic factor that affects ET_a and GR [40,54]. Therefore, to examine the climate seasonality at the study sites, mean monthly P and ET_p during the five-year study period are plotted in Figure 1. It can be seen from Figure 1 that the climates at the sites exhibited similar seasonal patterns with highest P and ET_p occurring during summer months. As such, it is reasonable to argue that climate seasonality did not exert a significant impact on the comparison of the distribution patterns of the simulated $\overline{ET_a}/\overline{P}$ and $\overline{GR}/\overline{P}$ across the sites in this study.
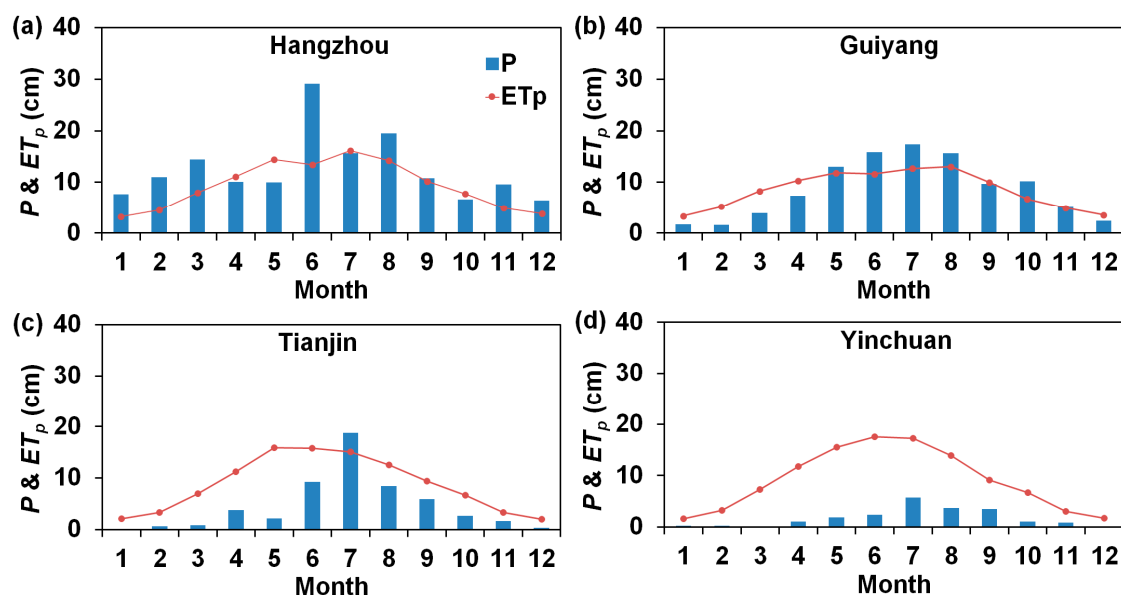

Figure 1. Mean monthly precipitation (P) and potential evapotranspiration (ET_p) during the study period at (**a**) Hangzhou, (**b**) Guiyang, (**c**) Tianjin, and (**d**) Yinchuan.

3.2. Simulated Patterns of MRD

To investigate the relationships of soil moisture with ET_a and GR on the basis of the *TSA* method, it is necessary to first examine whether simulated soil moisture data could mimic the field phenomenon of soil moisture temporal stability as shown in previous field studies. To this end, Figure 2 shows the ranked *MRD* with associated *SDRD* obtained for different soil textures at the study sites. As previously explained, only soil moisture data simulated at 25 cm were used to compute *MRD* and *SDRD* in Figure 2. In general, the simulated *MRD* patterns were similar to those derived from field observations at various spatiotemporal scales [20–24]. In particular, Figure 2 shows that certain samples displayed consistently wetter soil moisture conditions (i.e., with larger *MRD* values) than others. More importantly, the ranges of both *MRD* and *SDRD* were in line with previously reported values obtained at watershed and regional scales [24,53,55]. For example, the range of *MRD* for loamy sand was from −0.765 to 1.287 at Hangzhou, from −0.797 to 1.324 at Guiyang, from −0.819 to 1.237 at Tianjin, and from −0.912 to 1.166 at Yinchuan (Table 3). It should be emphasized that there were variations in the statistical characteristics of *MRD* and *SDRD* produced by different modeling studies [28,29], which could be largely attributed to

the differences in the synthetic soil hydraulic parameter datasets and hydrometeorological conditions used for simulations.
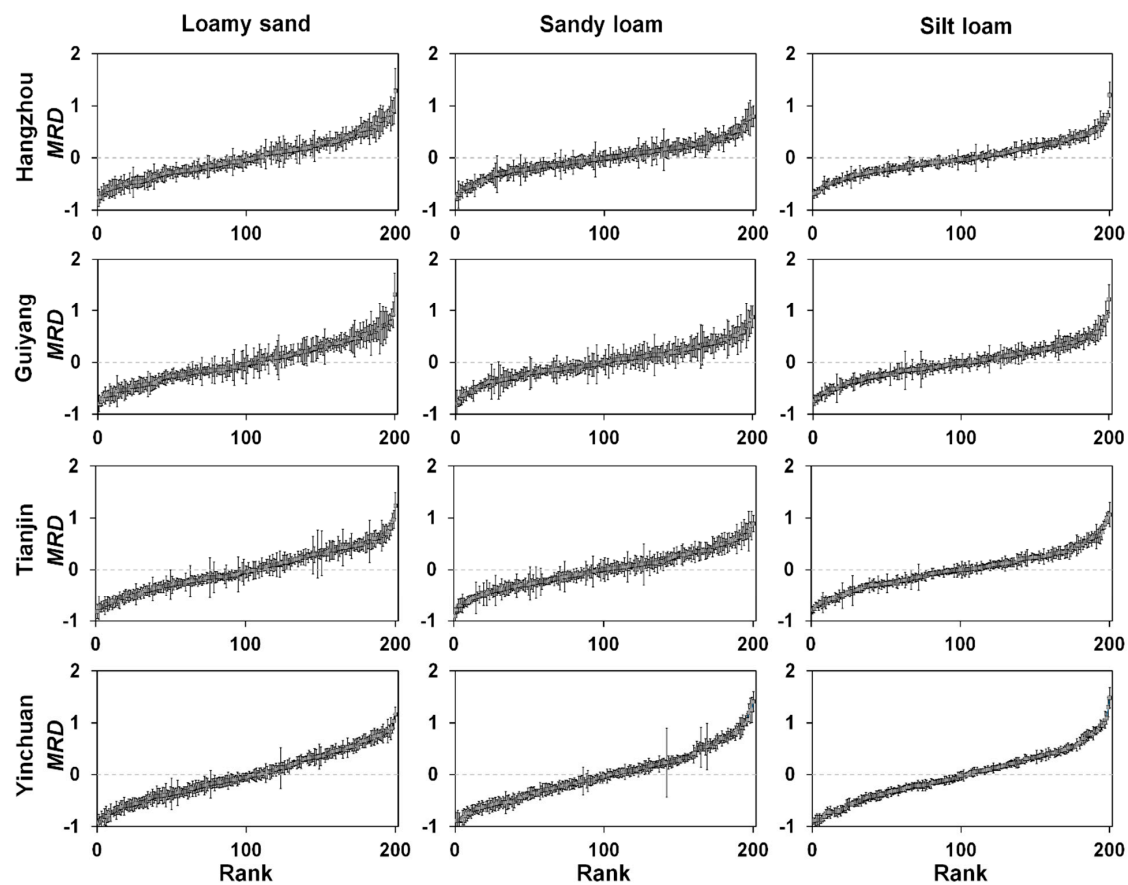

Figure 2. Ranked mean relative difference (*MRD*) of soil moisture with one standard deviation (vertical bars) for different soil textures at the study sites. Simulated soil moisture data at 25 cm were used to compute *MRD*.

Table 3. Statistical summary of mean relative difference (*MRD*) and standard deviation of relative difference (*SDRD*) of soil moisture. Simulated soil moisture data at 25 cm were used to compute *MRD* and *SDRD*.

Location	Loamy Sand			Sandy Loam			Silt Loam		
	Range of *MRD*	Range of *SDRD*	Mean *SDRD*	Range of *MRD*	Range of *SDRD*	Mean *SDRD*	Range of *MRD*	Range of *SDRD*	Mean *SDRD*
Hangzhou	−0.765–1.287	0.046–0.428	0.139	−0.741–0.799	0.041–0.402	0.131	−0.690–1.210	0.022–0.264	0.085
Guiyang	−0.797–1.324	0.037–0.486	0.158	−0.789–0.873	0.049–0.430	0.159	−0.732–1.230	0.027–0.370	0.112
Tianjin	−0.819–1.237	0.043–0.462	0.133	−0.977–0.891	0.053–0.397	0.134	−0.793–1.064	0.032–0.301	0.091
Yinchuan	−0.912–1.166	0.035–0.397	0.114	−0.889–1.410	0.043–0.664	0.111	−0.890–1.485	0.024–0.199	0.073

It is worth noting that inconsistent findings have been reported from previous studies regarding the environmental conditions and factors that mainly control soil moisture temporal stability. For example, there still exists a debate on whether soil moisture is temporally more stable under wetter or drier conditions [29,52,56]. In this study, the average soil moisture temporal stability as indicated by mean *SDRD* values varied noticeably among the sites (Table 3). It appears that soil moisture tended to be temporally more stable under both very wet (e.g., Hangzhou) and dry (e.g., Yinchuan) climatic conditions, while soil moisture temporal stability was lowest under intermediate climatic conditions (e.g., Guiyang). This result is in general agreement with the conclusion made by Lawrence and

Hornberger [48], who showed that the observed soil moisture variability peaked in temperature regions with intermediate moisture conditions. Soil moisture levels remain high in humid regions due to the constant P inputs, which results in less temporal dynamics of soil moisture. In contrast, because of infrequent rainfall events in arid regions, soil moisture is also temporally less dynamic. Thus, it leads to the lowest soil moisture temporal stability at the sites with intermediate climatic conditions (e.g., in sub-humid regions).

Table 3 also reveals that mean *SDRD* values differed for different soil textures under the same climatic condition. For example, mean *SDRD* values were comparably smaller for silt loam than those for loamy sand and sandy loam at all sites. Based on a theoretical framework, Vereecken et al. [30] showed that the variability in soil hydraulic parameters could significantly affect soil moisture variability. From Table 2, it can be seen that the lower mean *SDRD* values for silt loam were mostly due to the smaller variability in the parameters α and K_S. It, thus, corroborates our previous conjecture that the statistical characteristics of *MRD* and *SDRD* produced by synthetic modeling approaches are partly dependent on the variability in soil hydraulic parameters generated for simulations. In summary, the results from the *TSA* demonstrate the viability of using synthetic modeling approaches for reproducing reasonable spatiotemporal structures of soil moisture as observed in the fields.

3.3. Distribution Patterns of $\overline{ET_a}/\overline{P}$ and $\overline{GR}/\overline{P}$

Following Wang et al. [31], histograms of simulated $\overline{ET_a}/\overline{P}$ and $\overline{GR}/\overline{P}$, as shown in Figure 3, are used to discern the differences in the distribution patterns of $\overline{ET_a}/\overline{P}$ and $\overline{GR}/\overline{P}$ under different climatic conditions and for different soil textures. For the same soil texture, Figure 3 reveals that the ranges of $\overline{ET_a}/\overline{P}$ and $\overline{GR}/\overline{P}$ varied noticeably among the study sites. In particular, the distribution of $\overline{ET_a}/\overline{P}$ increased towards the higher end of the range between 0 and 100% with increasing climate dryness, and the distribution of $\overline{GR}/\overline{P}$ exhibited an opposite trend. This modeling result suggests that $\overline{ET_a}/\overline{P}$ becomes progressively larger while $\overline{GR}/\overline{P}$ grows gradually less important from humid to arid sites, which is consistent with the general understanding of the climate effect on ET_a and GR [57]. Rainfall water infiltrated into soils needs to first satisfy the atmospheric demand for ET_a before becoming GR. Thus, the opportunity for the infiltrated water to be evapotranspired is much higher under drier climatic conditions due to the higher atmospheric demands for evapotranspiration, resulting in the increasing trend in $\overline{ET_a}/\overline{P}$ with increasing climate dryness.

Although the respective ranges were similar for $\overline{ET_a}/\overline{P}$ and $\overline{GR}/\overline{P}$ under the same climatic conditions, there were noticeable variations in the distribution patterns of $\overline{ET_a}/\overline{P}$ and $\overline{GR}/\overline{P}$ for different soil textures (Figure 3). In the order of loamy sand, sandy loam, and silt loam, there were proportionally more samples with higher $\overline{ET_a}/\overline{P}$ (or lower $\overline{GR}/\overline{P}$) values towards the higher (or lower) end of the distribution ranges, most notably at the sites of Hangzhou, Guiyang, and Tianjin. It reflects the controls of soil hydraulic properties on ET_a and GR processes. Due to the higher infiltration capacities (e.g., Table 2 shows that K_s becomes gradually smaller from loamy sand to sandy loam and silt loam), coarser soils tend to produce lower $\overline{ET_a}/\overline{P}$ and higher $\overline{GR}/\overline{P}$ ratios [40,58]. Interestingly, at the site of Yinchuan with very dry climatic conditions, the contrast in the distribution patterns of $\overline{ET_a}/\overline{P}$ and $\overline{GR}/\overline{P}$ was less obvious among different soil textures. Regardless of soil textural differences, most of P becomes ET_a in arid regions due to the limited water supplies, which greatly weakens the dependence of ET_a and GR on soil hydraulic properties. It, thus, suggests that the controls of soil hydraulic properties on ET_a and GR vary with climatic conditions.
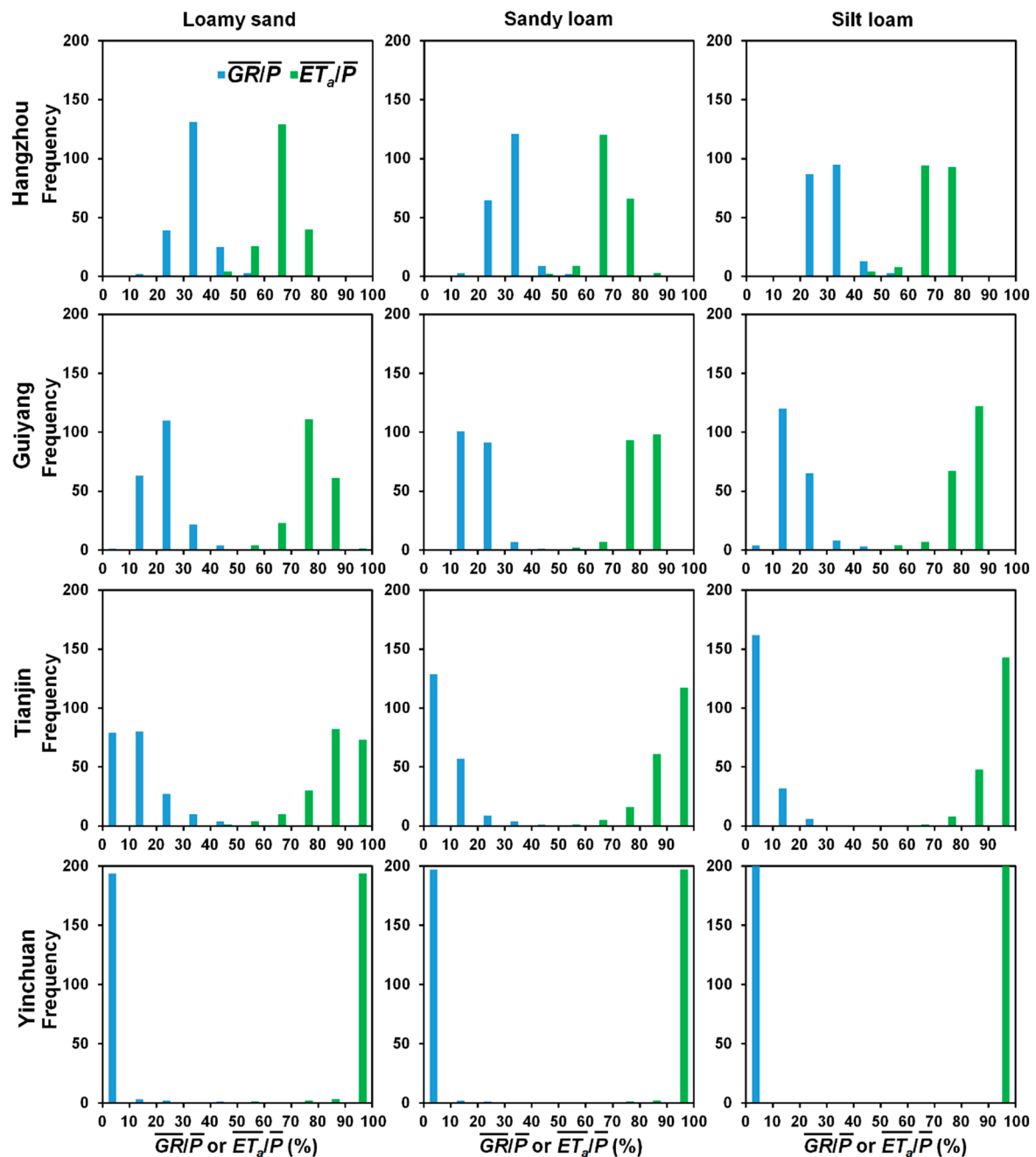
Figure 3. Distributions of simulated mean annual ratios of actual evapotranspiration ($\overline{ET_a}$) and groundwater recharge ($\overline{GR}$) over precipitation ($\overline{P}$).

3.4. Relationships of MRD with $\overline{ET_a}/\overline{P}$ and $\overline{GR}/\overline{P}$

To investigate the interplays between soil moisture and flux hydrological variables across vadose zones on the basis of the *TSA* method, the relationships between *MRD* and $\overline{ET_a}/\overline{P}$ are plotted in Figure 4 for the study sites. Note that due to the symmetry of the distributions of $\overline{ET_a}/\overline{P}$ and $\overline{GR}/\overline{P}$ (Figure 3), the relationships between *MRD* and $\overline{GR}/\overline{P}$ are not shown here for brevity. In addition, the non-parametric Spearman's rank correlation test was also carried out, and the correlation coefficients (r_p) of *MRD* with $\overline{ET_a}/\overline{P}$ and $\overline{GR}/\overline{P}$ are reported in Table 4. Overall, there existed positive correlations between *MRD* and $\overline{ET_a}/\overline{P}$, while negative ones between *MRD* and $\overline{GR}/\overline{P}$ (Table 4). The positive dependence of ET_a on soil moisture levels has been widely observed in the field [12,59]. Meanwhile, finer textured soils tend to have larger water holding capacities and lower *GR* [31], which leads to

higher soil moisture levels and *MRD* values for finer soils, and thus the negative correlation between *MRD* and *GR*.
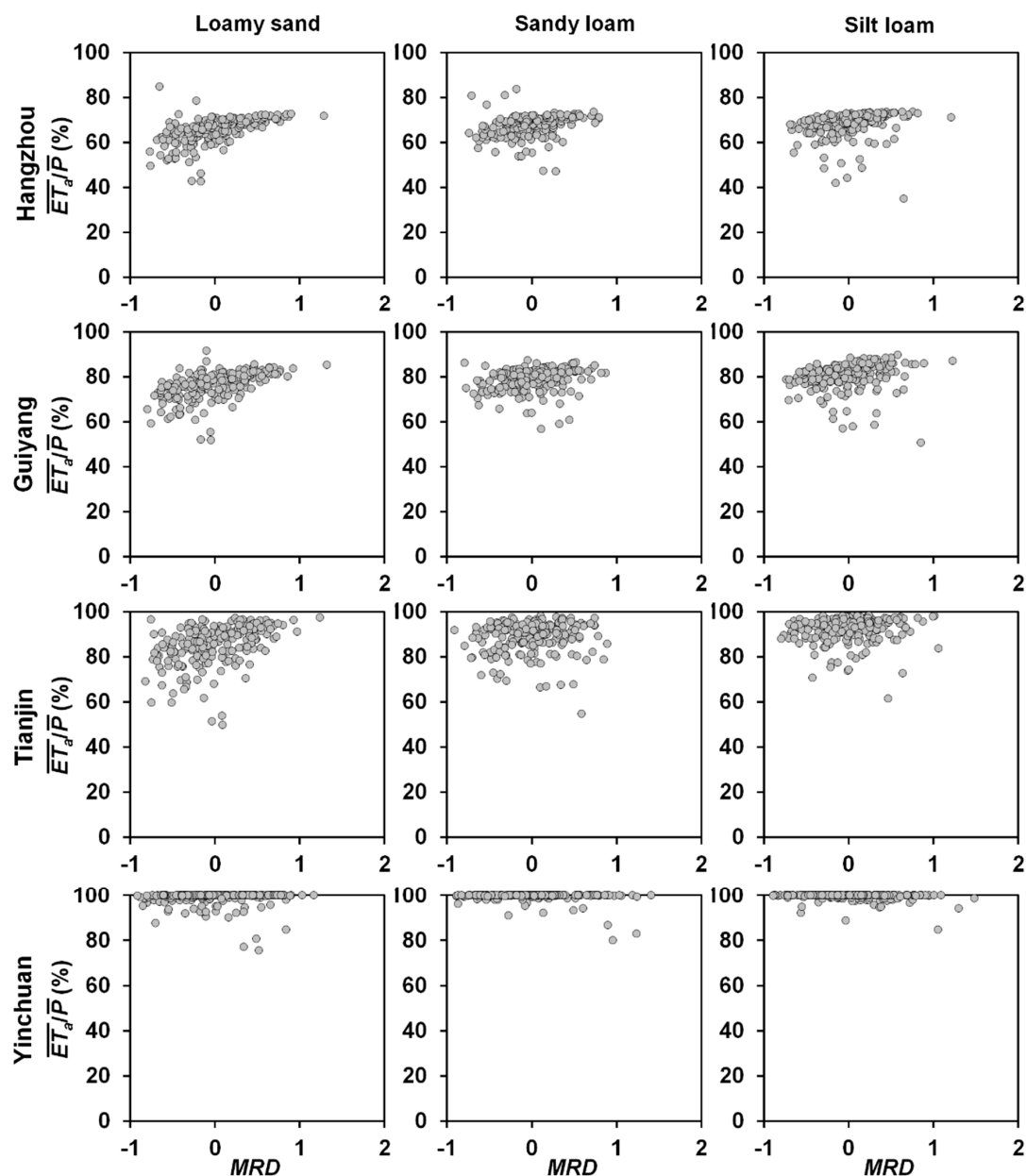

Figure 4. Relationships of mean relative difference (*MRD*) of soil moisture with mean annual ratio of actual evapotranspiration ($\overline{ET_a}$) over precipitation ($\overline{P}$).

More importantly, Figure 4 reveals that the ranges of *MRD* were similar at all sites for different soil textures; whereas, the ranges of $\overline{ET_a}/\overline{P}$ varied substantially across the sites. Specifically, the positive correlation between *MRD* and $\overline{ET_a}/\overline{P}$ was much stronger under wetter climatic conditions (e.g., Hangzhou and Guiyang) than under drier climatic conditions (e.g., Tianjin and Yinchuan; Table 4). In addition to climatic controls, soil hydraulic properties also play significant roles in affecting soil moisture levels, and thus *MRD*. As observed by Wang and Franz [9], the spatial distributions of *MRD* in Utah and the southeast United States were largely determined by soil hydraulic properties (most notably θ_r). Physically speaking, soil moisture levels cannot reach below θ_r under natural conditions. As such, regardless of climatic conditions, soil moisture levels might still vary considerably due to the variability in soil hydraulic properties (Figure 4). In contrast, as previously illustrated, the dependence

of ET_a on soil hydraulic properties greatly weakened under drier climatic conditions, leading to the smaller variability in $\overline{ET_a}/\overline{P}$ for different samples (e.g., at Yinchuan). To further demonstrate the varying dependence of *MRD* and $\overline{ET_a}/\overline{P}$ on soil hydraulic properties with climatic conditions, r_p of *MRD* and $\overline{ET_a}/\overline{P}$ with different soil hydraulic parameters was computed for sandy loam, and the results are reported in Table 5. It is clear from Table 5 that the control of θ_r on *MRD* greatly strengthened with increasing climate dryness, while the impacts of soil hydraulic properties on $\overline{ET_a}/\overline{P}$ along the gradient of increasing climate dryness was less obvious. Therefore, owing to the differences in the dependence of *MRD* and $\overline{ET_a}/\overline{P}$ on soil hydraulic properties, the correlation between *MRD* and $\overline{ET_a}/\overline{P}$ varied across different climate regimes. Moreover, Table 4 shows that the correlation between *MRD* and $\overline{ET_a}/\overline{P}$ was also dependent on soil texture. It appears that correlations between *MRD* and $\overline{ET_a}/\overline{P}$ were stronger for coarser soils (e.g., loamy sand) under the same climatic conditions, probably due to the tighter hydrological connection between vadose zone and land surface processes.

Table 4. Spearman's rank correlation coefficients of mean relative difference (*MRD*) of soil moisture with mean annual ratios of actual evapotranspiration ($\overline{ET_a}$) and groundwater recharge ($\overline{GR}$) over precipitation ($\overline{P}$).

Location	Loamy Sand		Sandy Loam		Silt Loam	
	$\overline{ET_a}/\overline{P}$	$\overline{GR}/\overline{P}$	$\overline{ET_a}/\overline{P}$	$\overline{GR}/\overline{P}$	$\overline{ET_a}/\overline{P}$	$\overline{GR}/\overline{P}$
Hangzhou	**0.679**	**−0.668**	**0.431**	**−0.429**	**0.461**	**−0.462**
Guiyang	**0.630**	**−0.623**	**0.288**	**−0.279**	**0.378**	**−0.393**
Tianjin	**0.482**	**−0.478**	0.123	−0.145 *	0.188 **	**−0.258**
Yinchuan	**0.255**	**−0.297**	0.227 **	**−0.241**	0.089	−0.158 *

* $p < 0.05$; ** $p < 0.01$; values in bold with $p < 0.001$.

Table 5. Spearman's rank correlation coefficients of soil hydraulic parameters for sandy loam with mean relative difference (*MRD*) of soil moisture and mean annual ratio of actual evapotranspiration ($\overline{ET_a}$) over precipitation ($\overline{P}$).

Soil Hydraulic Parameters	Hangzhou		Guiyang		Tianjin		Yinchuan	
	MRD	$\overline{ET_a}/\overline{P}$	*MRD*	$\overline{ET_a}/\overline{P}$	*MRD*	$\overline{ET_a}/\overline{P}$	*MRD*	$\overline{ET_a}/\overline{P}$
θ_r	**0.411**	**−0.372**	**0.573**	**−0.369**	**0.734**	**−0.356**	**0.920**	−0.018
θ_s	**0.497**	**0.481**	**0.398**	**0.422**	0.219 **	**0.351**	0.026	−0.095
α	−0.012	−0.176 *	0.026	**−0.307**	0.038	**−0.443**	0.061	**−0.493**
n	**−0.568**	**−0.270**	**−0.578**	**−0.351**	**−0.548**	**−0.363**	**−0.294**	−0.156 *
K_s	**−0.357**	**−0.406**	**−0.263**	**−0.301**	−0.109	−0.172 *	0.008	**0.286**

* $p < 0.05$; ** $p < 0.01$; values in bold with $p < 0.001$.

One of the main aims of the *TSA* method is to identify representative locations for measuring areal average moisture conditions [18]. Here, the criterion of *MRD* < ±0.05 was adopted to select representative samples with moisture conditions close to the average [60]. To examine whether the selected representative samples could also produce $\overline{ET_a}/\overline{P}$ values close to the average $\overline{ET_a}/\overline{P}$ of all samples (denoted as $\overline{ET_a}/\overline{P}^*$ hereafter), histograms of $\overline{ET_a}/\overline{P}$ associated with *MRD* < ±0.05 are shown in Figure 5 for different soil textures at the study sites. It can be seen from Figure 5 that the resulting number of representative samples with *MRD* < ±0.05 were different across the sites and for different soil textures. More importantly, although *MRD* only changed from −0.05 to 0.05 for the selected representative samples, associated $\overline{ET_a}/\overline{P}$ generally exhibited much wider ranges when compared to $\overline{ET_a}/\overline{P}^*$, except for at the site of Yinchuan. Due to the arid climate at Yinchuan, the spread of associated $\overline{ET_a}/\overline{P}$ was significantly reduced; thus, $\overline{ET_a}/\overline{P}^*$ corresponded well with the majority of associated

$\overline{ET_a}/\overline{P}$. Nevertheless, Figure 5 suggests that representative soil samples with moisture conditions close to the average as identified by the *TSA* method did not necessarily lead to representative soil samples for inferring $\overline{ET_a}/\overline{P}^*$, especially under wet climatic conditions.
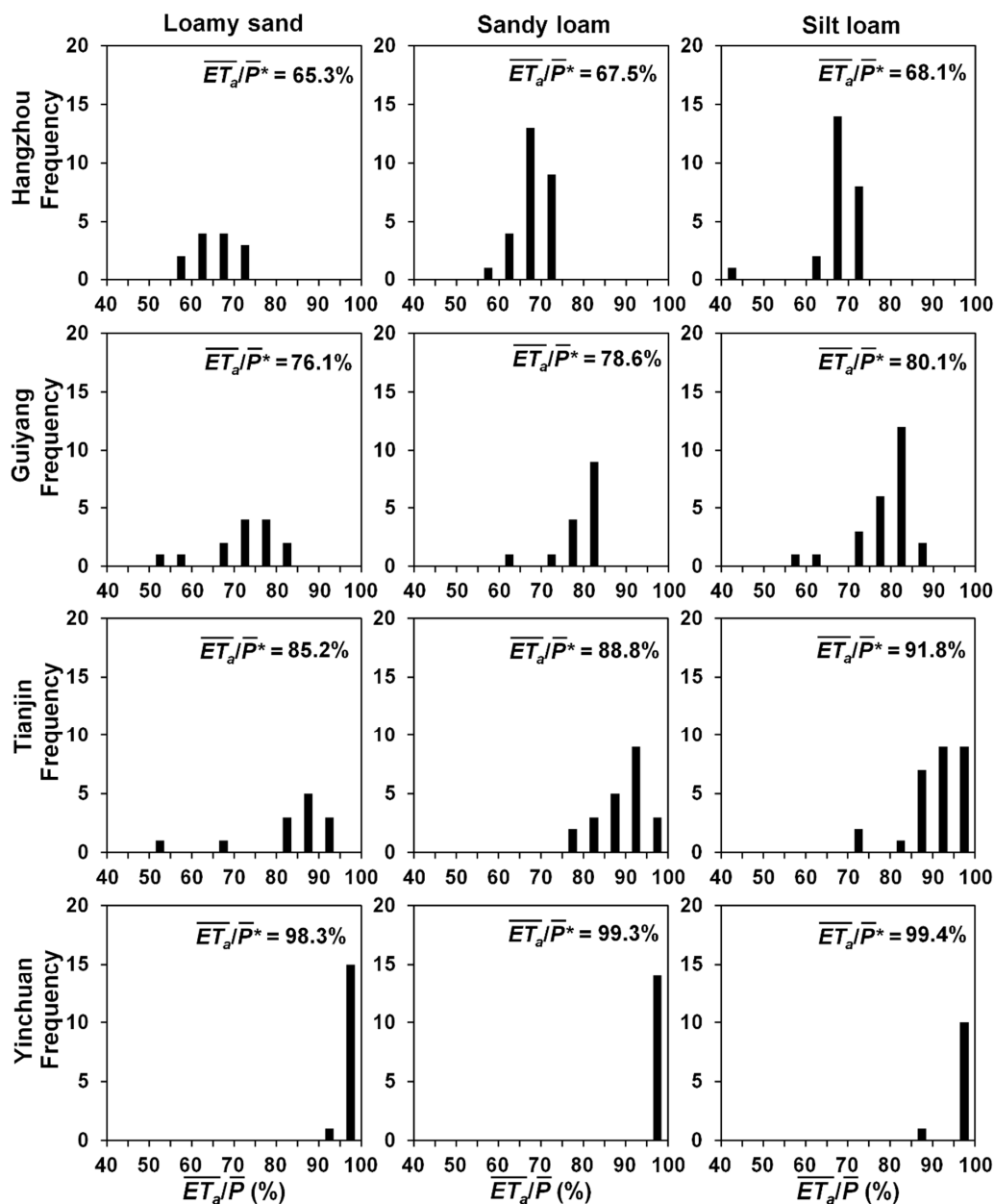

Figure 5. Distributions of mean annual ratio of actual evapotranspiration ($\overline{ET_a}$) over precipitation ($\overline{P}$). Samples with *MRD* < ±0.05 are used here to plot the distributions of $\overline{ET_a}/\overline{P}$. $\overline{ET_a}/\overline{P}^*$ is the average value of $\overline{ET_a}/\overline{P}$ from all samples.

With the aid of the *TSA* concept, the criterion of $(\overline{ET_a}/\overline{P} - \overline{ET_a}/\overline{P}^*) < \pm 0.01$ was used here for choosing representative samples with $\overline{ET_a}/\overline{P}$ close to $\overline{ET_a}/\overline{P}^*$. Using the same method as above, a similar result can be obtained, which shows that in spite of the use of the narrow range of $\overline{ET_a}/\overline{P}$ for selecting representative samples, the distributions of associated *MRD* with $(\overline{ET_a}/\overline{P} - \overline{ET_a}/\overline{P}^*) < \pm 0.01$ were much more scattered. It suggests that samples with average flux conditions might exhibit significant variability in soil moisture conditions.

To further reveal the correlations between average state and flux hydrological variables, an example is given in Figure 6, which shows the relationships of *MRD* and $\overline{ET_a}/\overline{P}$ with different soil hydraulic parameters for sandy loam at Guiyang. In the figure, samples with *MRD* < ±0.05 are highlighted. Part of the reason for the loose connection between average state and flux variables can be attributed to the complex interactions of *MRD* and $\overline{ET_a}/\overline{P}$ with soil hydraulic parameters, due to the high non-linearity of subsurface processes. Figure 6 shows that *MRD* from the representative samples was almost irrespective of θ_r, but associated $\overline{ET_a}/\overline{P}$ exhibited a clear negative relationship with θ_r. It is clear that samples with average moisture conditions generally do not correspond with samples with average $\overline{ET_a}/\overline{P}$ values, especially for the study sites with wet climatic conditions.
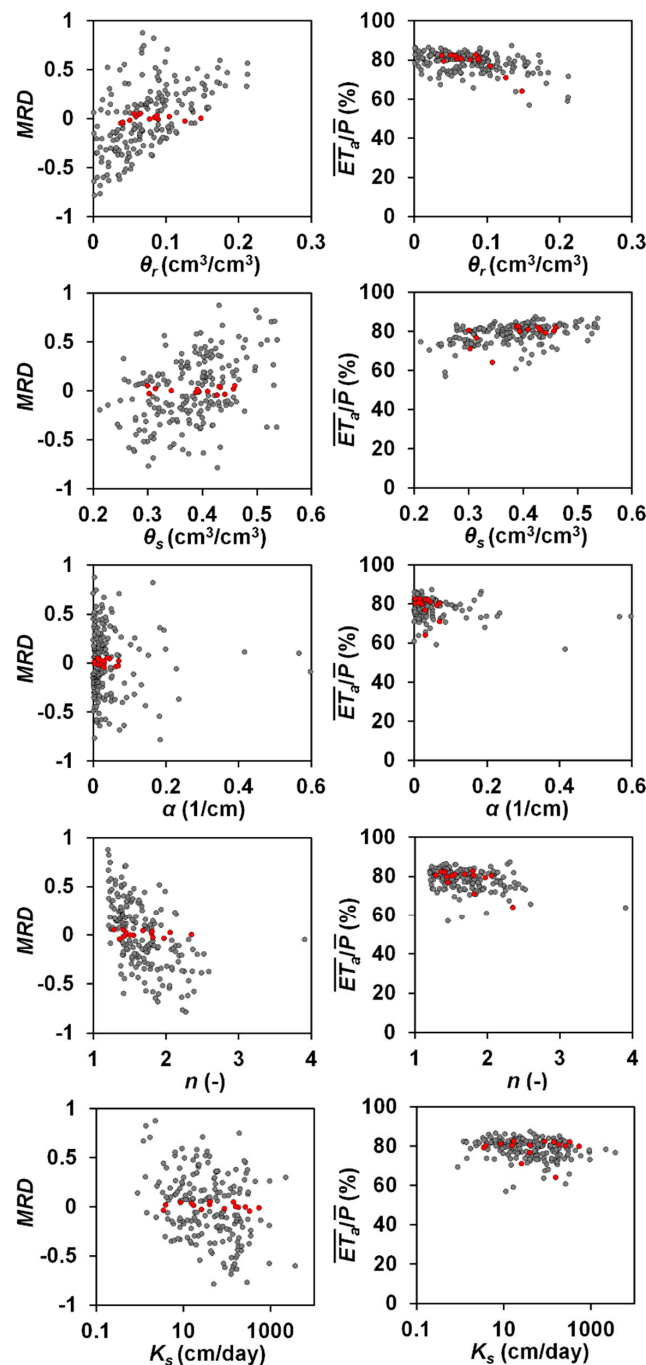
Figure 6. Relationships of *MRD* and $\overline{ET_a}/\overline{P}$ with different soil hydraulic parameters for sandy loam at Guiyang. Samples with *MRD* < ±0.05 are highlighted in red.

4. Conclusions

A synthetic modeling approach with generated soil hydraulic parameters was utilized in this study to investigate the interplays between state and flux hydrological variables across vadose zones in different climate zones. On the basis of the *TSA* method, reasonable soil moisture spatiotemporal structures were reproduced from the model. The simulation results revealed that although *MRD*, ET_a, and *GR* were affected by both climate and soil, their dependence on soil hydraulic properties varied considerably with climatic conditions. In particular, the controls of soil hydraulic properties on ET_a and *GR* greatly weakened under arid climatic conditions due to the limited water supplies, whereas the distribution of *MRD* still largely depended on soil hydraulic properties under the same climatic conditions. As such, the correlations of *MRD* with ET_a and *GR* varied with climatic conditions. Moreover, the modeling results showed that samples with average moisture conditions did not necessarily correspond with those with average flux conditions, which resulted from the complex interactions of soil moisture, ET_a, and *GR* with soil hydraulic properties. Although the *TSA* method has been widely used for selecting representative locations for monitoring areal average moisture conditions, the results of this study underscore the importance of using soil moisture information from multiple sites to infer areal average values of ET_a and *GR*, even with the knowledge of representative soil moisture monitoring sites.

References

1. Scanlon, B.R.; Keese, K.E.; Flint, A.L.; Flint, L.E.; Gaye, C.B.; Edmunds, W.M.; Simmers, I. Global synthesis of groundwater recharge in semiarid and arid regions. *Hydrol. Process.* **2006**, *20*, 3335–3370. [CrossRef]
2. Robinson, D.A.; Campbell, C.S.; Hopmans, J.W.; Hornbuckle, B.K.; Jones, S.B.; Knight, R.; Ogden, F.; Selker, J.; Wendroth, O. Soil moisture measurement for ecological and hydrological watershed-scale observatories: A review. *Vadose Zone J.* **2008**, *7*, 358–389. [CrossRef]
3. Wang, K.; Dickinson, R.E. A review of global terrestrial evapotranspiration: Observation, modeling, climatology, and climatic variability. *Rev. Geophys.* **2012**, *50*. [CrossRef]
4. Seneviratne, S.I.; Corti, T.; Davin, E.L.; Hirschi, M.; Jaeger, E.B.; Lehner, I.; Orlowsky, B.; Teuling, A.J. Investigating soil moisture–climate interactions in a changing climate: A review. *Earth-Sci. Rev.* **2010**, *99*, 125–161. [CrossRef]
5. Vereecken, H.; Huisman, J.A.; Pachepsky, Y.; Montzka, C.; van der Kruk, J.; Bogena, H.; Weihermüller, L.; Herbst, M.; Martinez, G.; Vanderborght, J. On the spatio-temporal dynamics of soil moisture at the field scale. *J. Hydrol.* **2014**, *516*, 76–96. [CrossRef]
6. Keese, K.E.; Scanlon, B.R.; Reedy, R.C. Assessing controls on diffuse groundwater recharge using unsaturated flow modeling. *Water Resour. Res.* **2005**, *41*. [CrossRef]
7. Szilagyi, J.; Zlotnik, V.A.; Gates, J.B.; Jozsa, J. Mapping mean annual groundwater recharge in the Nebraska Sand Hills, USA. *Hydrogeol. J.* **2011**, *19*, 1503–1513. [CrossRef]
8. Trambauer, P.; Dutra, E.; Maskey, S.; Werner, M.; Pappenberger, F.; van Beek, L.P.H.; Uhlenbrook, S. Comparison of different evaporation estimates over the African continent. *Hydrol. Earth Syst. Sci.* **2014**, *18*, 193–212. [CrossRef]
9. Wang, T.; Franz, T.E.; Zlotnik, V.A. Controls of soil hydraulic characteristics on modeling groundwater recharge under different climatic conditions. *J. Hydrol.* **2015**, *521*, 470–481. [CrossRef]
10. Daly, E.; Porporato, A. A review of soil moisture dynamics: From rainfall infiltration to ecosystem response. *Environ. Eng. Sci.* **2005**, *22*, 9–24. [CrossRef]

11. Kirchner, J.W. Getting the right answers for the right reasons: Linking measurements, analyses, and models to advance the science of hydrology. *Water Resour. Res.* **2006**, *42*. [CrossRef]

12. Vivoni, E.R.; Moreno, H.A.; Mascaro, G.; Rodriguez, J.C.; Watts, C.J.; Garatuza-Payan, J.; Scott, R.L. Observed relation between evapotranspiration and soil moisture in the North American monsoon region. *Geophys. Res. Lett.* **2008**, *35*. [CrossRef]

13. Peters-Lidard, C.D.; Clark, M.; Samaniego, L.; Verhoest, N.E.C.; van Emmerik, T.; Uijlenhoet, R.; Achieng, K.; Franz, T.E.; Woods, R. Scaling, similarity, and the fourth paradigm for hydrology. *Hydrol. Earth Syst. Sci.* **2017**, *21*, 3701–3713. [CrossRef] [PubMed]

14. Jung, M.; Reichstein, M.; Ciais, P.; Seneviratne, S.I.; Sheffield, J.; Goulden, M.L.; Bonan, G.; Cescatti, A.; Chen, J.; de Jeu, R.; et al. Recent decline in the global land evapotranspiration trend due to limited moisture supply. *Nature* **2010**, *467*, 951. [CrossRef]

15. Wang, T.; Franz, T.E.; Yue, W.; Szilagyi, J.; Zlotnik, V.A.; You, J.; Chen, X.; Shulski, M.D.; Young, A. Feasibility analysis of using inverse modeling for estimating natural groundwater recharge from a large-scale soil moisture monitoring network. *J. Hydrol.* **2016**, *533*, 250–265. [CrossRef]

16. Crow, W.T.; Berg, A.A.; Cosh, M.H.; Loew, A.; Mohanty, B.P.; Panciera, R.; de Rosnay, P.; Ryu, D.; Walker, J.P. Upscaling sparse ground-based soil moisture observations for the validation of coarse-resolution satellite soil moisture products. *Rev. Geophys.* **2012**, *50*. [CrossRef]

17. Liu, S.; Xu, Z.; Song, L.; Zhao, Q.; Ge, Y.; Xu, T.; Ma, Y.; Zhu, Z.; Jia, Z.; Zhang, F. Upscaling evapotranspiration measurements from multi-site to the satellite pixel scale over heterogeneous land surfaces. *Agric. For. Meteorol.* **2016**, *230–231*, 97–113. [CrossRef]

18. Vachaud, G.; Passerat De Silans, A.; Balabanis, P.; Vauclin, M. Temporal stability of spatially measured soil water probability density function1. *Soil Sci. Soc. Am. J.* **1985**, *49*, 822–828. [CrossRef]

19. Vanderlinden, K.; Vereecken, H.; Hardelauf, H.; Herbst, M.; Martínez, G.; Cosh, M.H.; Pachepsky, Y.A. Temporal stability of soil water contents: A review of data and analyses. *Vadose Zone J.* **2012**, *11*. [CrossRef]

20. Pachepsky, Y.A.; Guber, A.K.; Jacques, D. Temporal persistence in vertical distributions of soil moisture contents. *Soil Sci. Soc. Am. J.* **2005**, *69*, 347–352. [CrossRef]

21. Starr, G.C. Assessing temporal stability and spatial variability of soil water patterns with implications for precision water management. *Agric. Water Manag.* **2005**, *72*, 223–243. [CrossRef]

22. Guber, A.K.; Gish, T.J.; Pachepsky, Y.A.; van Genuchten, M.T.; Daughtry, C.S.T.; Nicholson, T.J.; Cady, R.E. Temporal stability in soil water content patterns across agricultural fields. *Catena* **2008**, *73*, 125–133. [CrossRef]

23. Brocca, L.; Melone, F.; Moramarco, T.; Morbidelli, R. Spatial-temporal variability of soil moisture and its estimation across scales. *Water Resour. Res.* **2010**, *46*. [CrossRef]

24. Wang, T.; Liu, Q.; Franz, T.E.; Li, R.; Lang, Y.; Fiebrich, C.A. Spatial patterns of soil moisture from two regional monitoring networks in the United States. *J. Hydrol.* **2017**, *552*, 578–585. [CrossRef]

25. Scanlon, B.R.; Healy, R.W.; Cook, P.G. Choosing appropriate techniques for quantifying groundwater recharge. *Hydrogeol. J.* **2002**, *10*, 18–39. [CrossRef]

26. Turkeltaub, T.; Kurtzman, D.; Bel, G.; Dahan, O. Examination of groundwater recharge with a calibrated/validated flow model of the deep vadose zone. *J. Hydrol.* **2015**, *522*, 618–627. [CrossRef]

27. Foolad, F.; Franz, T.E.; Wang, T.; Gibson, J.; Kilic, A.; Allen, R.G.; Suyker, A. Feasibility analysis of using inverse modeling for estimating field-scale evapotranspiration in maize and soybean fields from soil water content monitoring networks. *Hydrol. Earth Syst. Sci.* **2017**, *21*, 1263–1277. [CrossRef]

28. Martínez, G.; Pachepsky, Y.A.; Vereecken, H. Temporal stability of soil water content as affected by climate and soil hydraulic properties: A simulation study. *Hydrol. Process.* **2014**, *28*, 1899–1915. [CrossRef]

29. Wang, T. Modeling the impacts of soil hydraulic properties on temporal stability of soil moisture under a semi-arid climate. *J. Hydrol.* **2014**, *519*, 1214–1224. [CrossRef]

30. Vereecken, H.; Kamai, T.; Harter, T.; Kasteel, R.; Hopmans, J.; Vanderborght, J. Explaining soil moisture variability as a function of mean soil moisture: A stochastic unsaturated flow perspective. *Geophys. Res. Lett.* **2007**, *34*. [CrossRef]

31. Wang, T.; Zlotnik, V.A.; Šimunek, J.; Schaap, M.G. Using pedotransfer functions in vadose zone models for estimating groundwater recharge in semiarid regions. *Water Resour. Res.* **2009**, *45*. [CrossRef]

32. Simunek, J.; Sejna, M.; Saito, H.; Sakai, M.; van Genuchten, M.T. *The HYDRUS-1 D Software Package for Simulating the One-Dimensional Movement of Water, Heat, and Multiple Solutes in Variably-Saturated Media*; Version 4.17; Depart. of Environ. Sci., University of California Riverside: Riverside, CA, USA, 2013; p. 308.

33. Zlotnik, V.A.; Wang, T.; Nieber, J.L.; Šimunek, J. Verification of numerical solutions of the Richards equation using a traveling wave solution. *Adv. Water Resour.* **2007**, *30*, 1973–1980. [CrossRef]

34. Neuman, S.P.; Feddes, R.A.; Bresler, E. *Finite Element Simulation of Flow in Saturated-Unsaturated Soils Considering Water Uptake by Plants*; Third Annual Report; Proj. A10-SWC-77; Hydraul. Eng. Lab., Technion: Haifa, Israel, 1974.

35. Feddes, R.A.; Kowalik, P.J.; Neuman, S.P. *Simulation of Field Water Use and Crop Yield*; John Wiley and Sons: New York, NY, USA, 1978.

36. Ritchie, J.T. Model for predicting evaporation from a row crop with incomplete cover. *Water Resour. Res.* **1972**, *8*, 1204–1213. [CrossRef]

37. Wang, T.; Zlotnik, V.A. A complementary relationship between actual and potential evapotranspiration and soil effects. *J. Hydrol.* **2012**, *456–457*, 146–150. [CrossRef]

38. Myneni, R.B.; Hoffman, S.; Knyazikhin, Y.; Privette, J.L.; Glassy, J.; Tian, Y.; Wang, Y.; Song, X.; Zhang, Y.; Smith, G.R.; et al. Global products of vegetation leaf area and fraction absorbed PAR from year one of MODIS data. *Remote Sens. Environ.* **2002**, *83*, 214–231. [CrossRef]

39. Jackson, R.B.; Canadell, J.; Ehleringer, J.R.; Mooney, H.A.; Sala, O.E.; Schulze, E.D. A global analysis of root distributions for terrestrial biomes. *Oecologia* **1996**, *108*, 389–411. [CrossRef]

40. Small, E.E. Climatic controls on diffuse groundwater recharge in semiarid environments of the southwestern United States. *Water Resour. Res.* **2005**, *41*. [CrossRef]

41. Available online: http://www.ncdc.noaa.gov/cdo-web/ (accessed on 19 June 2019).

42. Hargreaves, G.H.; Samani, Z.A. Estimation potential evapotranspiration. *J. Irrig. Drain. Eng. ASCE* **1982**, *108*, 223–230.

43. Gutiérrez-Jurado, H.A.; Vivoni, E.R.; Harrison, J.B.J.; Guan, H. Ecohydrology of root zone water fluxes and soil development in complex semiarid rangelands. *Hydrol. Process.* **2006**, *20*, 3289–3316. [CrossRef]

44. Vogel, T.; Dohnal, M.; Dusek, J.; Votrubova, J.; Tesar, M. Macroscopic modeling of plant water uptake in a forest stand involving root-mediated soil water redistribution. *Vadose Zone J.* **2013**, *12*. [CrossRef]

45. Wesseling, J.G. *Meerjarige Simulatie van Grondwaterstroming voor Verschillende Bodemprofielen, Grondwatertrappen en Gewassen Met Het Model SWATRE*. Rapport 152; Wageningen, DLO-Staring Centrum. 1991, p. 63. Available online: https://library.wur.nl/WebQuery/wurpubs/fulltext/304226 (accessed on 19 June 2019).

46. Mualem, Y. A new model for predicting the hydraulic conductivity of unsaturated porous media. *Water Resour. Res.* **1976**, *12*, 513–522. [CrossRef]

47. Van Genuchten, M.T. A closed-form equation for predicting the hydraulic conductivity of unsaturated soils. *Soil Sci. Soc. Am. J.* **1980**, *44*, 892–898. [CrossRef]

48. Lawrence, J.E.; Hornberger, G.M. Soil moisture variability across climate zones. *Geophys. Res. Lett.* **2007**, *34*. [CrossRef]

49. Teuling, A.J.; Hupet, F.; Uijlenhoet, R.; Troch, P.A. Climate variability effects on spatial soil moisture dynamics. *Geophys. Res. Lett.* **2007**, *34*. [CrossRef]

50. Zhang, Y.; Schaap, M.G. Weighted recalibration of the Rosetta pedotransfer model with improved estimates of hydraulic parameter distributions and summary statistics (Rosetta3). *J. Hydrol.* **2017**, *547*, 39–53. [CrossRef]

51. Zhang, Y.; Schaap, M.G.; Guadagnini, A.; Neuman, S.P. Inverse modeling of unsaturated flow using clusters of soil texture and pedotransfer functions. *Water Resour. Res.* **2016**, *52*, 7631–7644. [CrossRef]

52. Martínez-Fernández, J.; Ceballos, A. Temporal stability of soil moisture in a large-field experiment in Spain. *Soil Sci. Soc. Am. J.* **2003**, *67*, 1647–1656. [CrossRef]

53. Wang, T.; Franz, T.E. Field observations of regional controls of soil hydraulic properties on soil moisture spatial variability in different climate zones. *Vadose Zone J.* **2015**, *14*. [CrossRef]

54. Yokoo, Y.; Sivapalan, M.; Oki, T. Investigating the roles of climate seasonality and landscape characteristics on mean annual and monthly water balances. *J. Hydrol.* **2008**, *357*, 255–269. [CrossRef]

55. Cosh, M.H.; Jackson, T.J.; Moran, S.; Bindlish, R. Temporal persistence and stability of surface soil moisture in a semi-arid watershed. *Remote Sens. Environ.* **2008**, *112*, 304–313. [CrossRef]

56. Zhao, Y.; Peth, S.; Wang, X.Y.; Lin, H.; Horn, R. Controls of surface soil moisture spatial patterns and their temporal stability in a semi-arid steppe. *Hydrol. Process.* **2010**, *24*, 2507–2519. [CrossRef]

57. Zhang, L.; Dawes, W.R.; Walker, G.R. Response of mean annual evapotranspiration to vegetation changes at catchment scale. *Water Resour. Res.* **2001**, *37*, 701–708. [CrossRef]

58. Wang, T.; Istanbulluoglu, E.; Lenters, J.; Scott, D. On the role of groundwater and soil texture in the regional water balance: An investigation of the Nebraska Sand Hills, USA. *Water Resour. Res.* **2009**, *45*. [CrossRef]

59. Chen, X.; Rubin, Y.; Ma, S.; Baldocchi, D. Observations and stochastic modeling of soil moisture control on evapotranspiration in a Californian oak savanna. *Water Resour. Res.* **2008**, *44*. [CrossRef]

60. Hu, W.; Shao, M.; Han, F.; Reichardt, K.; Tan, J. Watershed scale temporal stability of soil water content. *Geoderma* **2010**, *158*, 181–198. [CrossRef]